ELSEVIER

Biophysical Chemistry 132 (2008) 81–88

Biophysical Chemistry

http://www.elsevier.com/locate/biophyschem

Investigating the binding of curcumin derivatives to bovine serum albumin

Bijaya Ketan Sahoo, Kalyan Sundar Ghosh, Swagata Dasgupta *

Department of Chemistry, Indian Institute of Technology, Kharagpur 721302, India

Received 10 September 2007; received in revised form 14 October 2007; accepted 14 October 2007
Available online 23 October 2007

Abstract

The interaction of bovine serum albumin (BSA) with isoxazolcurcumin (IOC) and diacetylcurcumin (DAC) has been investigated. Binding constants obtained were found to be in the 10^5 M^{-1} range. Minor conformational changes of BSA were observed from circular dichroism (CD) and Fourier transformed infrared (FT-IR) studies on binding. Based on Förster's theory of non-radiation energy transfer, the average binding distance, r between the donor (BSA) and acceptors IOC and DAC was found to be 3.79 and 4.27 nm respectively. Molecular docking of isoxazolcurcumin and diacetylcurcumin with bovine serum albumin indicated that they docked close to Trp 213, which is within the hydrophobic subdomain.

Keywords: Bovine serum albumin; Isoxazolcurcumin; Diacetylcurcumin; UV–Visible; Conformational studies; Docking

1. Introduction

Curcumin is a natural product found in the rhizome of *Curcuma longa*. Ongoing research and clinical trials provide ample evidence that this natural phenolic compound possesses diverse pharmacological potencies. Besides its effective anti-oxidant, antidiabetic, anti-inflammatory and antimicrobial/antiviral properties [1], the compound is also considered as a cancer chemo-preventive agent [2,3]. A number of derivatives of curcumin are also widely used as antibacterial, anti-protozoal, anti-angiogenic and anti-cancer agents [4,5]. The interaction of curcumin with human serum albumin (HSA) and bovine serum albumin (BSA) has been investigated [6–10] but curcumin derivatives have not been studied in detail. In this report we have looked at the interactions of isoxazole and diacetyl derivatives of curcumin with BSA primarily because of the potent activities of the two derivatives.

Isoxazole derivatives are known to exhibit antibacterial, antifungal, anti-inflammatory, anticonvulsant, antiviral and immunological activities and a few of them have also found clinical application as drugs [11]. Isoxazole has also been used as a scaffold for constructing highly functionalized molecules to bind with folded DNA conformations [12]. Isoxazolcurcumin (IOC) (Scheme 1A) is anti-inflammatory and like curcumin acts as a strong antioxidant [13]. The replacement of the β-diketo fragment of curcumin in IOC exhibits significantly higher inhibitory activity towards the COX-2 enzyme compared to curcumin [13]. IOC is also known to have modest inhibitory activity against HIV-1 and HIV-2 Proteases [14].

Diacetylcurcumin (DAC) (Scheme 1B) shows better anti-bacterial activity than curcumin against multiresistant bacteria [15], has strong nitric oxide (NO) scavenging activity [16] and can pass through the blood-brain barrier to exhibit a suppressing effect on NO levels *in vivo* [17]. DAC possesses scavenging activity against $O_2^{\cdot -}$ anion and can also prevent neurotoxicity [18,19]. The DAC complex formed with Fe (III) has greater stability than the curcumin complex [20] due to its greater basicity. This is of practical importance because of its role in oxygen transport, electron transfer and DNA synthesis.

Human and bovine serum albumins are the most abundant plasma carrier proteins contributing significantly to physiological functions [21–23]. They have been widely used as models to gain insight into protein-ligand binding [23,24]. BSA is a 583-residue protein structurally homologous to HSA consisting of three homologous all-α domains [25–27]. BSA has two tryptophans (Trp 134 and Trp 213), of which Trp 213 has been

* Corresponding author. Tel.: +91 3222 283306; fax: +91 3222 255303.
E-mail address: swagata@chem.iitkgp.ernet.in (S. Dasgupta).

0301-4622/$ - see front matter © 2007 Elsevier B.V. All rights reserved.
doi:10.1016/j.bpc.2007.10.007

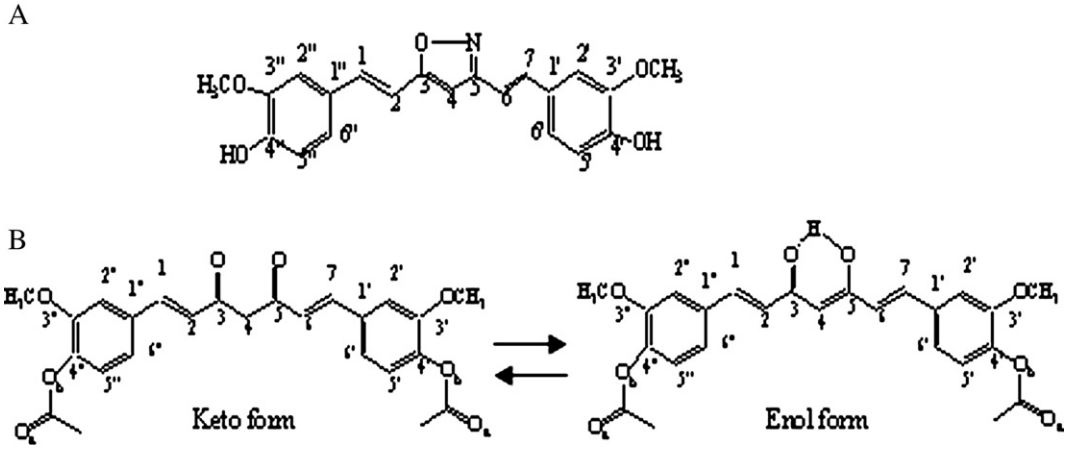

Scheme 1. Structures of (A) isoxazolcurcumin (IOC) and (B) diacetylcurcumin (DAC).

proposed to be located in a cleft or in a hydrophobic fold like Trp 214 in HSA whereas the additional tryptophan residue of BSA (Trp 134) has been proposed to be on the surface of the molecule [28,29].

The observed increase in activity of IOC and DAC with respect to curcumin makes the study of their interactions with BSA worthy of investigation. We have looked into the interaction of IOC and DAC with BSA by UV–Visible, CD, FT-IR spectroscopy and determined the energy transfer between the donor Trp residues in BSA to the ligands by calculation of the Förster distance. These observations were substantiated by docking studies.

2. Experimental

2.1. Materials

BSA, curcumin (mixture) and warfarin were from Sigma (USA). All other reagents of analytical grade were from SRL India. Pure curcumin was separated from the mixture by a silica gel column. IOC and DAC were synthesized from pure curcumin according to the methods in [14] and [18] respectively and characterization data compared with the available literature [14,18,30]. NMR (^{1}H and ^{13}C) spectra were recorded on a Bruker AC 200 MHz instrument (δ scale) in $CDCl_3$ using trimethylsilane (TMS) as the internal standard. IR spectra (KBr pelleted) were recorded on a Perkin Elmer RX I spectrometer. BSA, IOC and DAC concentrations were determined spectroscopically using molar absorption coefficients of 43,800 M^{-1} cm^{-1} for BSA at 280 nm [31], 40,268 M^{-1} cm^{-1}at 339 nm (IOC) and 42,246 M^{-1} cm^{-1} at 399 nm (DAC). The latter two values were determined as follows: Absorbance values of several dilutions of a stock solution of IOC and DAC, prepared in ethanol, because of their relative insolubility in water, were measured at the respective absorption maxima. The absorption coefficients were calculated from the slope of a plot of absorbance vs. concentration. All experiments were performed in 10 mM phosphate buffer pH 7 with ethanol not exceeding 5%.

2.2. UV–Visible

UV measurements were made using a Perkin Elmer spectrophotometer (Model Lambda 25) at 25 °C. Titrations were performed in a 1 cm quartz cuvette by successive addition of BSA (0 to 15 μM) to a 3 ml solution of IOC (15 μM) and DAC (10 μM) in phosphate buffer containing ethanol.

2.3. Circular dichroism and FT-IR measurements

CD measurements were carried out on a Jasco-810 automatic recording spectropolarimeter at 25 °C. Solutions were prepared by mixing a fixed concentration of BSA (9 μM) with varying concentrations of IOC and DAC in aqueous ethanol (2.5%) to have protein:ligand molar ratios ranging from 1:1 to 1:4. Solutions were scanned at 0.1 cm and 1 cm path length from 190–240 and 300–500 nm respectively under nitrogen flow. Scan rates of 50 nm/min and 100 nm/min were used for 190–240 and 300–500 nm respectively with a response time of 4 s. The CD response obtained was expressed in terms of mean residue ellipticity (MRE) in deg cm^2 $dmol^{-1}$ using Eq. (1) [32].

$$\mathrm{MRE} = \frac{\mathrm{observedCD(mdeg)}}{C_p \times n \times l \times 10} \tag{1}$$

where C_p is the molar concentration of the protein, n is the number of amino acid residues in the protein (583) and l is the path length (0.1 cm). The α-helical content of free and complexed BSA was calculated from the MRE values at 208 nm [32,33] by using Eq. (2).

$$\begin{aligned} \alpha\text{-}Helix(\%) &= \frac{(-\mathrm{MRE}_{208} - 4000)}{33,000 - 4000} \times 100 \\ &= \frac{(-\mathrm{MRE}_{208} - 4000)}{29,000} \times 100 \end{aligned} \tag{2}$$

where MRE_{208} corresponds to the observed MRE values, 33,000 and 4000 are the MRE values of a pure α-helix and of the β-form and random coil conformation at 208 nm respectively.

FT-IR measurements were carried out at room temperature on a Nexus-870 FT-IR spectrometer (Thermo Nicolet Corporation). A stock solution of BSA (24 μM) in buffer was prepared. IOC and DAC in aqueous ethanol were mixed with BSA in a 1:1 molar ratio. Higher molar ratios of IOC and DAC could not be used due to insolubility and precipitation. 20 μl of the sample mixture was placed between a pair of CaF_2 discs (32 mm diameter) and spectra collected by a 128-scan interferogram in a single beam mode with a resolution of 4 cm^{-1}. The spectrometer was continuously purged with dry air. Control spectra were collected under the same conditions.

2.4. Fluorescence resonance energy transfer (FRET)

Fluorescence emission was carried out at 25 °C on a Spex Fluorolog-3 Spectrofluorimeter. The bandwidth of both excitation and emission slits were 5 nm with an integration time of 0.2 s. For 1:1 molar ratio the fluorescence quenching were performed in a 1 cm quartz cuvette by addition IOC and DAC to a 3 ml solution of BSA in phosphate buffer. To minimize the inner filter effect a low concentration of BSA (2 μM) with absorbance value of 0.02 [34] was used and checked by using; $F_{corr}=F_{obs}\times$antilog $[(OD_{ex}+OD_{em})/2]$ [34] where F_{corr} and F_{obs} are the corrected and observed fluorescence intensities. For warfarin displacement 0.5 μM BSA was used. Control spectra were recorded for each sample measurement.

Energy transfer occurs when the fluorescence emission spectrum of the donor and absorption spectrum of the acceptor have suitable overlap and the donor and the acceptor are within the characteristic Förster distance [34]. The efficiency of energy transfer, E, is calculated using Eq. (3) [34].

$$E = 1 - \frac{F}{F_0} = \frac{R_0^6}{R_0^6 + r^6} \tag{3}$$

where F and F_0 are the fluorescence intensities of BSA in the presence and absence of the ligand, r is the distance between donor and acceptor and R_0 is the critical distance when the energy transfer efficiency is 50%. The value of R_0 is calculated using Eq. (4).

$$R_0 = 9.78 \times 10^3 \left[\left(\kappa^2 n^{-4} Q_D J(\lambda)\right)\right]^{\frac{1}{6}} \text{ in Å} \tag{4}$$

where κ^2 is the relative orientation in space of the transition dipoles of the donor and acceptor, n is the refractive index of the medium, Q_D the fluorescence quantum yield of the donor in absence of acceptor and J the overlap integral of the fluorescence emission spectrum of the donor and the absorption spectrum of the acceptor given by Eq. (5) [34].

$$J = \frac{\int F_D(\lambda)\varepsilon_A(\lambda)\lambda^4 d\lambda}{\int F_D(\lambda) d\lambda} \tag{5}$$

where $F_D(\lambda)$ is dimensionless and is the corrected fluorescence intensity of the donor in the wavelength range λ to $\lambda+\Delta\lambda$ with the total intensity (area under the curve) normalized to unity. $\varepsilon_A(\lambda)$, in units of M^{-1} cm^{-1}, is the extinction coefficient of the acceptor at λ.

2.5. Molecular docking and accessible surface area calculations

A homology model of BSA was used for the docking studies with IOC and DAC since the structure is unavailable in the Protein Data Bank [35]. A BLAST search in the PDB with a BSA sequence [Swissprot sequence ALBU_BOVIN (P02769)] revealed 75% identity with HSA. The SAM_T06 server was used to obtain the model structure [36–40]. Energy minimized structures of IOC and the enol form of DAC were generated by Sybyl 6.92 (Tripos Inc., St. Louis, USA) with the help of the MMFF94 force field using MMFF94 charges. FlexX available in the Sybyl suite was used for the docking of IOC and the enol form of DAC to BSA. PyMol [41] was used for visualization of the docked conformations.

The accessible surface area (ASA) of BSA (uncomplexed) and its docked complex with both IOC and DAC were calculated using NACCESS [42]. The protein-ligand structure corresponding to the minimum score as obtained from the FlexX analysis was chosen and composite coordinates of the complex generated. The change in ASA for residue, i was calculated using $\Delta ASA^i = ASA^i_{BSA} - ASA^i_{BSA\text{-}ligand}$. If a residue lost more than 10 $Å^2$ ASA when going from the uncomplexed to the complexed state it was considered as being involved in the interaction.

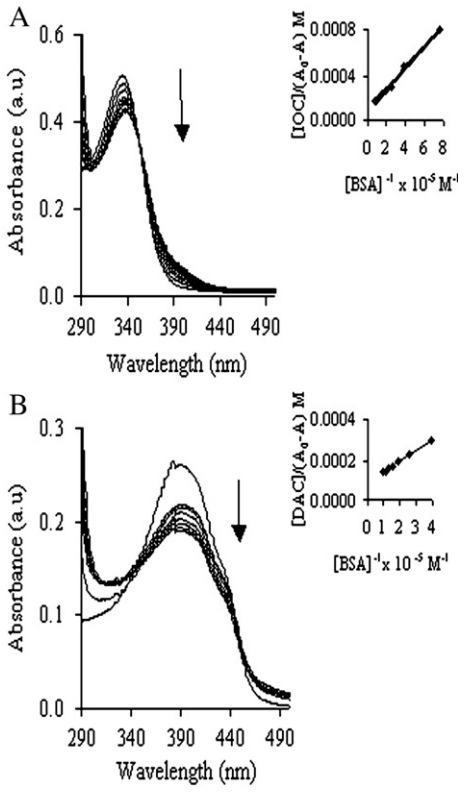

Fig. 1. Absorption spectra of IOC (15 μM) and DAC (10 μM) in absence (top) and presence of BSA (0–15 μM) in phosphate buffer pH=7.0. The arrow indicates increasing [BSA]. Inset: Double reciprocal plot of the corresponding binding system.

3. Results and discussion

3.1. UV–Vis spectral studies

DAC undergoes keto-enol tautomerism (Scheme 1B) due to the presence of the β-diketone moiety. This allows extended conjugation between the π-electron systems of the two feruloyl type chromophores resulting in a conjugated π-system like curcumin that has its absorption maximum at 429 nm [8]. The absorption band for DAC is observed in the visible region with a maximum at 400 nm in aqueous ethanol. For IOC, due to the incorporation of the isoxazole ring, the planarity of the central methylene carbon is lost. This disrupts the extended conjugation between the two feruloyl moieties, so the absorption maximum of IOC is observed at 339 nm. An analogous situation arises when a bulky substituent is present on the central methylene carbon atom that sterically prevents the molecule from adopting a planar geometry. In this case also the λ_{max} shifts to the near-ultraviolet region [43].

Fig. 1 shows the absorption spectrum of IOC and DAC in 10 mM phosphate buffer (pH 7) in absence and presence of varying concentrations of BSA. On addition of BSA to IOC and DAC, the change in absorbance values at 335 nm (BSA-IOC system) and 392 nm (BSA-DAC system) were monitored. Isobestic points observed at 344 and 447 nm for DAC and 303 and 352 nm for IOC are indicative of complex formation. Considering a simple equilibrium binding system, a quantitative estimation for the binding was obtained from Eq. (6) [44], where the equilibrium constant of complex formation was calculated from changes in absorbance values at a fixed wavelength.

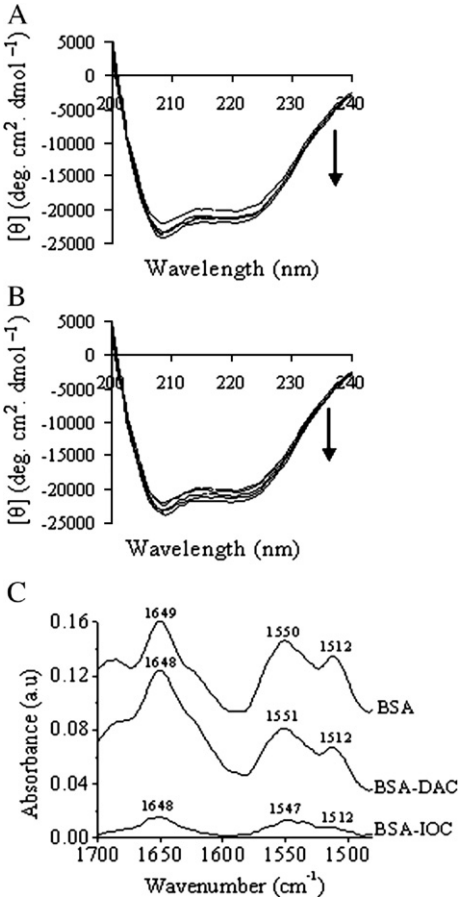

Fig. 2. CD spectra of BSA in absence and presence of (A) IOC and (B) DAC; [BSA]=9 μM; [IOC] and [DAC]=9 μM to 36 μM. The arrow indicates increasing [IOC] and [DAC]. (C) FT-IR difference spectra of BSA [(BSA in buffer)-(buffer)], BSA-IOC [(BSA+IOC)−(IOC)] and BSA-DAC [(BSA+DAC)−(DAC)].

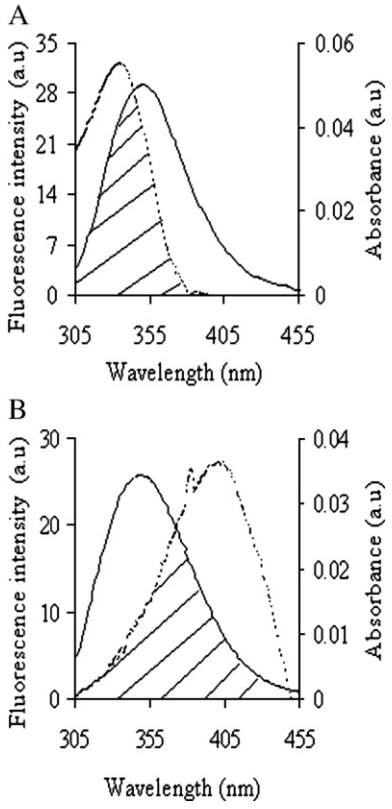

Fig. 3. Spectral overlap between the fluorescence emission spectrum of BSA (solid line) and absorption spectrum of (A) IOC and (B) DAC in phosphate buffer pH=7.0. [Ligand]:[BSA]=1:1; λ_{ex}=295 nm.; λ_{em}=349 nm.

$$\frac{[L_0]}{A} = \frac{1}{\varepsilon} + \frac{1}{\varepsilon K[M]} \tag{6}$$

where ε is the extinction coefficient of the complex, $[L_0]$ the initial molar concentration of the ligand (IOC or DAC), $[M]$ is the concentration of BSA and A is the absorbance due to complex formation. The ratio of the intercept to the slope of the double reciprocal plots for BSA-IOC (inset Fig. 1A) and BSA-DAC (inset Fig. 1B) between $[L_0]/A$ versus $1/[M]$ gives the association/binding constant (K) of complex formation. The binding constant obtained for the BSA-IOC complex was $3.17 \pm 0.58 \times 10^5$ M^{-1} and that for the BSA-DAC complex $1.31 \pm 0.20 \times 10^5$ M^{-1}. The higher value for the BSA-IOC complex is indicative of a stronger association. The values are in the same range of curcumin binding with BSA [6].

3.2. Circular dichroism and Fourier transform infrared studies

The CD spectra of BSA in the absence and presence of IOC and DAC are shown in Fig. 2. BSA exhibits two negative bands

in the far UV region at 208 and 222 nm characteristic of α-helices [45]. The α-helix content of free BSA (60±2.0%) is within the range observed in other studies [46]. The increase in the α-helical content to 67±2.6% and 66±1.5% in presence of IOC and DAC respectively can be attributed to conformational adjustments on complex formation. No induced CD was found by adding BSA to IOC and DAC independently from 300–500 nm under the experimental conditions.

The protein amide I band at 1650–1654 cm^{-1} (due to C═O stretching) and amide II band at 1548–1560 cm^{-1} (C–N stretch coupled with N–H bending mode) are related to the secondary structure of proteins [47]. The observed peak shifts of the amide I and amide II regions in the FT-IR spectrum, albeit minor, are a little higher in BSA-IOC than in BSA-DAC (Fig. 2(C)). This indicates that IOC probably causes a slightly larger conformational perturbation compared to DAC.

3.3. Energy transfer between BSA and IOC/DAC

The spectral overlap between the fluorescence emission spectrum of BSA and the UV absorption spectra of the ligands is shown in Fig. 3. J values calculated by integrating the overlap area of the spectra from 305 to 384 nm and 305 to 449 nm, were found to be 1.99×10^{-14} M^{-1} cm^3 for IOC and 1.76×10^{-14} M^{-1} cm^3 for DAC. Using, $\kappa^2=2/3$, $n=1.336$ and $Q_D=0.15$ [48], R_0 calculated from Eq. (4) was 2.84 nm and 2.78 nm for IOC and DAC respectively. The value of r obtained for IOC was 3.79 nm from Eq. (3) using $E=0.151$ calculated from fluorescence data. Similar values for DAC were 4.27 nm and 0.072 respectively. The donor-to-acceptor distance lies within the range of $0.5R_0$ to $2R_0$ [34] in each case indicating efficient energy transfer from BSA to both ligands. This implies that one or both Trp residues are in close proximity to IOC and DAC. The distance, r is the average value between bound ligands and the two tryptophan residues [49]. The relatively smaller value for r and higher value for E of IOC is indicative of a closer association and possibly higher perturbation of the structure, which is what is observed from the experimental studies. Of the two tryptophans in BSA, Trp 213 is located in a hydrophobic fold whereas Trp-134 is located on the surface of the molecule [29]. The lipophilic nature of the ligands indicates that they would preferentially bind to the hydrophobic subdomain of BSA. To corroborate this speculation, docking studies along with warfarin (marker of drug site I of subdomain

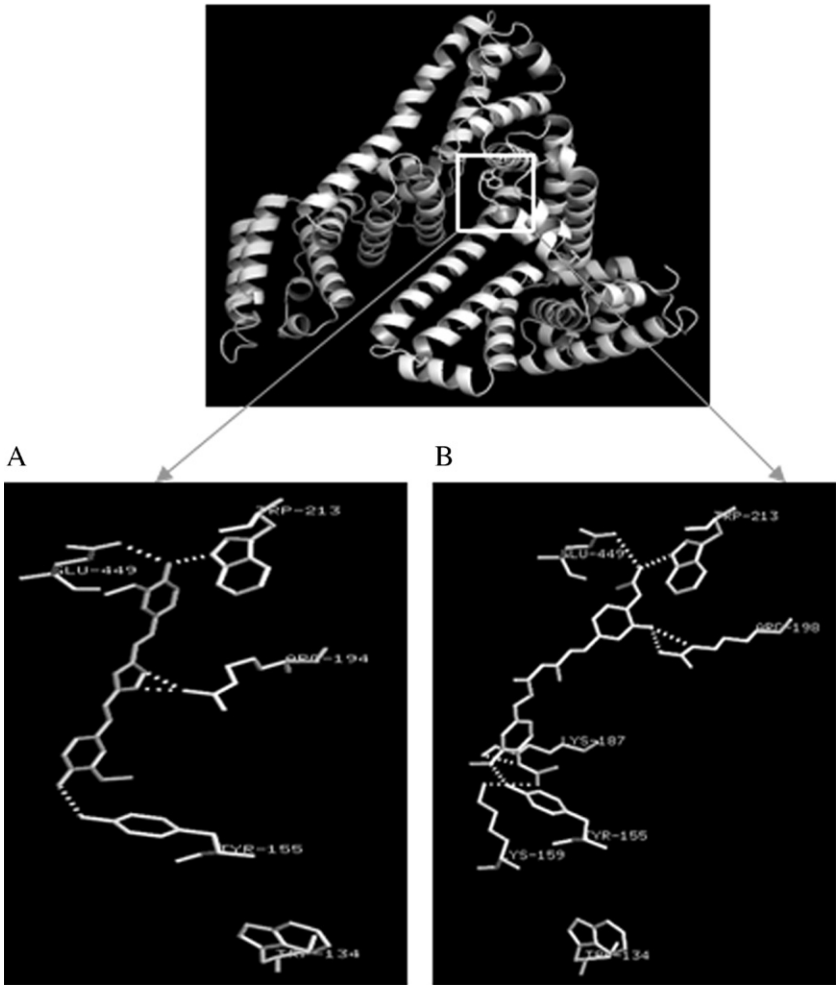

Fig. 4. Schematic representation of docked conformation of (A) IOC and (B) DAC (enol form) with interacting residues of BSA. Trp 213 is shown within the box in the cartoon representation of BSA (top).

Table 1
Distances (in Ångströms) between polar neighbors of BSA with IOC and DAC

BSA	IOC	DAC (enol form)
Tyr 155 O	2.88 [4′-O]	2.84 [3′-O]
Lys 159 N		3.38 [4′-O_b]
Lys 187 N		3.00 [4′-O_b]
Arg 194 Nη1	2.12 [3-O]	
Arg 194 Nη1	2.33 [5-N]	
Arg 198 Nη1		2.79 [3″-O]
Arg 198 N		3.15 [3″-O]
Trp 213 N	2.71 [4″-O]	2.84 [4″-O_a]
Glu 449 O	2.70 [4″-O]	3.28 [4″-O_a]

IIA in HSA) displacement studies with HSA and BSA by IOC and DAC were performed.

4. Docking results

The docking pose of IOC and DAC (enol form) with BSA indicate that both IOC and DAC dock to hydrophobic subdomain as shown in Fig. 4. In IOC, the oxygen atoms at 4′, 4″, 3 and nitrogen atom at 5 positions are within hydrogen bonding distance of Tyr 155, Arg 194, Trp 213, and Glu 449. Similarly for DAC, the oxygen atoms at 3′, 3″, 4′ and 4″ positions are within hydrogen bonding distance from Tyr 155, Lys 159, Lys 187, Arg 198, Trp 213, and Glu 449 as tabulated in Table 1. The involvement of Tyr is also observed in the FT-IR difference spectra attributed to the peak at 1512 cm^{-1} (Fig. 2(C)) because tyrosine residues are associated with a sharp band at 1515 cm^{-1} [50,51]. The change in accessible surface area (ΔASA) after binding was calculated and shown in Table 2. It was found that the ΔASA of Trp 213 is >25 $Å^2$ indicating its probable involvement in complex formation. This tentatively suggests that the preferential binding site for the ligands is close to Trp 213 as is expected.

4.1. Warfarin displacement by IOC and DAC

Warfarin is known to bind to drug site I of subdomain II A of HSA [52,53]. Warfarin itself has a weak fluorescence, which is enhanced on binding to HSA. The fluorescence intensity of bound warfarin to HSA is reduced if a second ligand competes for the same site in the protein. As Trp 213 in BSA is in a hydrophobic fold like Trp 214 in HSA (subdomain II A) [28,29], the accessibility of Trp 213 in BSA can be confirmed by comparing the displacement of HSA and BSA bound warfarin by the ligands IOC and DAC. Fig. 5 shows the displacement of BSA bound warfarin by IOC and DAC, which is similar to the case of HSA (Fig. 5 inset). Competition studies with BSA bound warfarin indicate that both IOC and DAC displace warfarin thus confirming the binding of these ligands to subdomain II A in BSA. This justifies the preferential accessibility of the ligands to Trp 213 rather than Trp 134 in BSA similar to Trp 214 of HSA.

Table 2
Change in accessible surface area (ΔASA) in $Å^2$ of interacting residues of BSA (uncomplexed), and its complex with IOC and DAC

Amino acid residue	ΔASA ($Å^2$) (BSA-IOC)	ΔASA ($Å^2$) (BSA-DAC)
Trp 134	0.0	0.0
Tyr 155	28.8	34.4
Tyr 156	11.7	11.9
Lys 159	3.2	13.1
Lys 187	32.6	41.2
Arg 194	64.8	50.4
Trp 213	26.9	26.1
Arg 217	27.3	30.8
Glu 291	43.1	65.2
Val 342	12.0	4.2
Glu 449	15.2	10.6
Asp 450	65.6	53.8
Ser 453	20.7	19.2

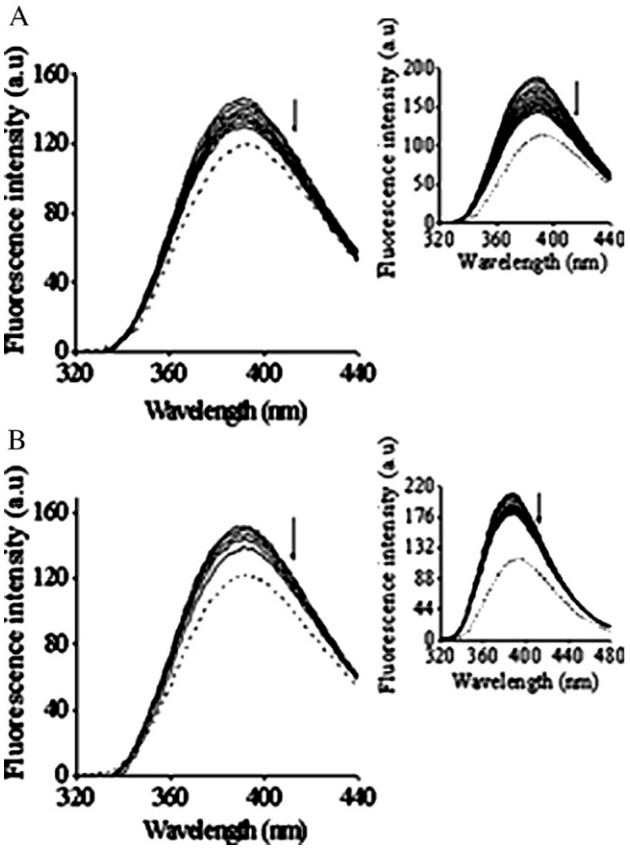

Fig. 5. Displacement of BSA bound warfarin (0.5 μM) by (A) IOC and (B) DAC. [IOC or DAC]=0 to 1 μM; λ_{ex}=308 nm and λ_{ex}=388 nm. Inset: Displacement of HSA bound warfarin (0.5 μM) by (A) IOC and (B) DAC; [IOC]=0 to 1.7 μM; [DAC]=0 to 2.9 μM. Dotted spectra correspond to warfarin alone.

5. Conclusion

The interaction studies of IOC and DAC with BSA indicate a stronger association with IOC compared to DAC. An investigation of the structure reveals the loss of planarity due to the incorporation of the isoxazole ring that disrupts the extended conjugation possible in curcumin and DAC. This preliminary study with curcumin derivatives provides promise in the design of potential candidates that could associate more

strongly to the serum albumins. Here we find that the binding of IOC and DAC in BSA occurs in the hydrophobic cleft and preferentially near Trp 213. Similar studies with HSA are near completion with the thermodynamics involved in the association for both proteins also under investigation.

Acknowledgements

The authors are grateful to Central Research Facility, IIT Kharagpur for experimental studies. The authors wish to thank Professor Kevin Karplus for help in obtaining the structure of BSA. BKS is thankful to the All India Council for Technical Education (AICTE) for fellowship.

References

[1] V.S. Govindarajan, Turmeric — chemistry, technology and quality, CRC Crit. Rev. Food Sci. Nutr. 12 (1980) 199–310.
[2] B.B. Aggarwal, A. Kumar, A.C. Bharti, Anticancer potential of curcumin: preclinical and clinical studies, Anticancer Res. 23 (2003) 363–398.
[3] D.P. Chauhan, Chemotherapeutic potential of curcumin for colorectal cancer, Curr. Pharm. Des. 8 (2002) 1695–1706.
[4] C.V. Rao, A. Rivenson, B. Simi, B.S. Reddy, Chemoprevention of colon carcinogenesis by dietary curcumin, a naturally occurring plant phenolic compound, Cancer Res. 55 (1995) 259–266.
[5] J.L. Arbiser, N. Klauber, R. Rohn, R.V. Leeuwen, M.T. Huang, C. Fisher, E. Flynn, H.R. Byers, Curcumin is an *in vivo* inhibitor of angiogenesis, Mol. Med. 4 (1998) 376–383.
[6] A. Barik, K.I. Priyadarsini, H. Mohan, Photophysical studies on binding of curcumin to bovine serum albumins, Photochem. Photobiol. 77 (2003) 597–603.
[7] A.C. Pulla Reddy, E. Sudharshan, A.G. Appu Rao, B.R. Lokesh, Interaction of curcumin with human serum albumin — a spectroscopic study, Lipids 34 (1999) 1025–1029.
[8] F. Zsila, Z. Bikádi, M. Simonyi, Unique, pH-dependent biphasic band shape of the visible circular dichroism of curcumin-serum albumin complex, Biochem. Biophys. Res. Commun. 301 (2003) 776–782.
[9] A. Barik, B. Mishra, A. Kunwar, K.I. Priyadarsini, Interaction of curcumin with human serum albumin: thermodynamic properties, fluorescence energy transfer and denaturation effects, Chem. Phys. Lett. 436 (2007) 239–243.
[10] A. Kunwar, A. Barik, R. Pandey, K.I. Priyadarsini, Transport of liposomal and albumin loaded curcumin to living cells: an absorption and fluorescence spectroscopic study, Biochim. Biophys. Acta 1760 (2006) 1513–1520.
[11] A. Jezierska, J. Panek, S. Ryng, DFT study of a novel lead structure in the isoxazole heterocyclic system, J. Mol. Struct. (Theocem) 636 (2003) 203–214.
[12] X. Han, C. Li, K.C. Rider, A. Blumenfeld, B. Twamley, N.R. Natale, The isoxazole as a linchpin for molecules that target folded DNA conformations: selective lateral lithiation and palladation, Tetrahedron Lett. 43 (2002) 7673–7677.
[13] C. Selvam, S.M. Jachak, R. Thilagavathi, A.K. Chakraborti, Design, synthesis, biological evaluation and molecular docking of curcumin analogues as antioxidant, cyclooxygenase inhibitory and anti-inflammatory agents, Bioorg. Med. Chem. Lett. 15 (2005) 1793–1797.
[14] Z. Sui, R. Salto, J. Li, C. Craik, P.R. Ortiz de Montellano, Inhibition of the HIV-1 and HIV-2 proteases by curcumin and curcumin boron complexes, Bioorg. Med. Chem. 1 (1993) 415–422.
[15] S. Mishra, U. Narain, R. Mishra, K. Misra, Design, development and synthesis of mixed bioconjugates of piperic acid–glycine, curcumin–glycine/alanine and curcumin–glycine– piperic acid and their antibacterial and antifungal properties, Bioorg. Med. Chem. 13 (2005) 1477–1486.
[16] Y. Sumanont, Y. Murakami, M. Tohda, O. Vajragupta, K. Matsumoto, H. Watanabe, Evaluation of the nitric oxide radical scavenging activity of manganese complexes of curcumin and its derivative, Biol. Pharm. Bull. 27 (2004) 170–173.
[17] Y. Sumanont, Y. Murakami, M. Tohda, O. Vajragupta, H. Watanabe, K. Matsumoto, Prevention of kainic acid-induced changes in nitric oxide level and neuronal cell damage in the rat hippocampus by manganese complexes of curcumin and diacetylcurcumin, Life Sci. 78 (2006) 1884–1891.
[18] O. Vajragupta, P. Boonchoong, H. Watanabe, M. Tohda, N. Kummasud, Y. Sumanont, Manganese complexes of curcumin and its derivatives: evaluation for the radical scavenging ability and neuroprotective activity, Free Radic. Biol. Med. 35 (2003) 1632–1644.
[19] O. Vajragupta, P. Boonchoong, L.J. Berliner, Manganese complexes of curcumin analogues: evaluation of hydroxyl radical scavenging ability, superoxide dismutase activity and stability towards hydrolysis, Free Radic. Res. 38 (2004) 303–314.
[20] M. Borsari, E. Ferrari, R. Grandi, M. Saladini, Curcuminoids as potential new iron-chelating agents: spectroscopic, polarographic and potentiometric study on their Fe(III) complexing ability, Inorg. Chim. Acta 328 (2002) 61–68.
[21] U. Kragh-hansen, Molecular aspects of ligand binding to serum albumin, Pharmacol. Rev. 33 (1981) 17–53.
[22] T. Peters, Serum albumin, Adv. Protein Chem. 37 (1985) 161–245.
[23] D.C. Carter, J.X. Ho, Structure of serum albumin, Adv. Protein Chem. 45 (1994) 153–203.
[24] S.M.T. Shaikh, J. Seetharamappa, S. Ashoka, P.B. Kandagal, Spectroscopic studies and life time measurements of binding of a bioactive compound to bovine serum albumin and the effects of common ions and other drugs on binding, Chem. Pharm. Bull. 54 (2006) 422–427.
[25] D.C. Carter, B. Chang, J.X. Ho, K. Keeling, Z. Krishnasami, Preliminary crystallographic studies of four crystal forms of serum albumin, Eur. J. Biochem. 226 (1994) 1049–1052.
[26] X.M. He, D.C. Carter, Atomic structure and chemistry of human serum albumin, Nature 358 (1992) 209–215.
[27] M. Dockal, D.C. Carter, F. R¨uker, Conformational transitions of the three recombinant domains of human serum albumin depending on pH, J. Biol. Chem. 275 (2000) 3042–3050.
[28] S. Sugio, A. Kashima, S. Mochizuki, M. Noda, K. Kobayashi, Crystal structure of human serum albumin at 2.5 Å resolution, Protein Eng. 12 (1999) 439–446.
[29] B.F. Peterman, K.J. Laidler, Study of reactivity of tryptophan residues in serum albumins and lysozyme by N-bromosuccinamide fluorescence quenching, Arch. Biochem. Biophys. 199 (1980) 158–164.
[30] P.J. Roughley, D.A. Whiting, Experiments in the biosynthesis of curcumin, J. Chem. Soc., Perkin Trans 1 (1973) 2379–2388.
[31] C.N. Pace, F. Vajdos, L. Fee, G. Grimsley, T. Gray, How to measure and predict the molar absorption coefficient of a protein, Protein Sci. 4 (1995) 2411–2423.
[32] G. Hong, L. Lei, J. Liu, Q. Kong, X. Chen, Z. Hu, The study on the interaction between human serum albumin and a new reagent with antitumour activity by spectrophotometric methods, J. Photochem. Photobiol., A Chem. 167 (2004) 213–221.
[33] Y-H. Chen, J.T. Yang, H.M. Martinez, Determination of the secondary structures of proteins by circular dichroism and optical rotatory dispersion, Biochemistry 11 (1972) 4120–4131.
[34] J.R. Lakowicz, Principles of Fluorescence Spectroscopy, Springer, New York, 2006.
[35] H.M. Berman, J. Westbrook, Z. Feng, G. Gilliland, T.N. Bhat, H. Weissig, I.N. Shindyalov, P.E. Bourne, The Protein Data Bank, Nucleic Acids Res. 28 (2000) 235–242.
[36] K. Karplus, S. Katzman, G. Shackleford, M. Koeva, J. Draper, B. Barnes, M. Soriano, R. Hughey, SAM-T04: what's new in protein-structure prediction for CASP6, Proteins 61 (2005) 135–142.
[37] R. Karchin, M. Cline, K. Karplus, Evaluation of local structure alphabets based on residue burial, Proteins 55 (2004) 508–518.
[38] R. Karchin, M. Cline, Y. Mandel-Gutfreund, K. Karplus, Hidden Markov models that use predicted local structure for fold recognition: alphabets of backbone geometry, Proteins 51 (2003) 504–514.
[39] R. Karchin, J. Draper, J. Casper, Y. Mandel-Gutfreund, M. Diekhans, R. Hughey, Combining local-structure, fold-recognition, and new-fold methods for protein structure prediction, Proteins 53 (2003) 491–496.

[40] K. Karplus, R. Karchin, C. Barrett, S. Tu, M. Cline, M. Diekhans, L. Grate, J. Casper, R. Hughey, What is the value added by human intervention in protein structure prediction? Proteins 45 (2001) 86–91.
[41] W.L. Delano, The PyMOL Molecular Graphics System, DeLano Scientific, San Carlos CA, USA, 2004 http://pymol.sourceforge.net/.
[42] S.J. Hubbard, J.M. Thornton, 'NACCESS', Computer Program, Department of Biochemistry and Molecular Biology, University College, London, 1993.
[43] U. Pedersen, P.B. Rasmussen, S.O. Lawesson, Synthesis of naturally occurring curcuminoids and related-compounds, Liebigs Ann. Chem. 8 (1985) 1557–1569.
[44] H.A. Benesi, J.H. Hildebrand, A Spectrophotometric Investigation of the Interaction of Iodine with Aromatic Hydrocarbons, J. Am. Chem. Soc. 71 (1949) 2703–2707.
[45] M.G. Gore, Spectrophotometry and Spectrofluorimetry. A Practical approach, Oxford University Press, New York, 2000.
[46] R.G. Reed, R.C. Feldhoff, O.L. Clute, T. Peters Jr., Fragments of Bovine serum albumin produced by limited proteolysis. Conformation and ligand binding, Biochemistry 14 (1975) 4578–4583.
[47] D.M. Byler, H. Susi, Examination of the secondary structure of proteins by deconvolved FT-IR spectra, Biopolymers 25 (1986) 469–487.
[48] F.L. Cui, J. Fan, J.P. Li, Z. Hu, Interactions between 1-benzoyl-4-p-chlorophenyl thiosemicarbazide and serum albumin: investigation by fluorescence spectroscopy, Bioorg. Med. Chem. 12 (2004) 151–157.
[49] J. Liu, J. Tian, J. Zhang, Z. Hu, X. Chen, Interaction of magnolol with bovine serum albumin: A fluorescence-quenching study, Anal. Bioanal. Chem. 376 (2003) 864–867.
[50] H. Susi, D.M. Byler, Protein structure by Fourier transform infrared spectroscopy: second derivative spectra, Biochem. Biophys. Res. Commun. 115 (1983) 391–397.
[51] H. Susi, D.M. Byler, Resolution-enhanced Fourier transform infrared spectroscopy of enzymes, Methods Enzymol. 130 (1986) 290–311.
[52] G. Sudlow, D.J. Birkett, D.N. Wade, The characterization of two specific drug binding sites on human serum albumin, Mol. Pharmacol. 11 (1975) 824–832.
[53] I. Petitpas, A.A. Bhattacharya, S. Twine, M. East, S. Curry, Crystal structure analysis of warfarin binding to human serum albumin: anatomy of drug site I, J. Biol. Chem. 276 (2001) 22804–22809.